Article:

Liu, E, Yu, H-S, Deng, G et al. (2 more authors) (2014) Numerical analysis of seepage–deformation in unsaturated soils. Acta Geotechnica, 9 (6). pp. 1045-1058. ISSN 1861-1125

https://doi.org/10.1007/s11440-014-0343-y

Numerical Analysis of the Seepage-Deformation in Unsaturated Soils

Enlong Liu[1*], Hai-Sui Yu[2], Gang Deng[3], Jianhai Zhang[1], Siming He[4]

[1] State Key Laboratory of Hydraulics and Natural River Engineering, College of Water Resource and Hydropower, Sichuan University, Chengdu, P.R. China 610065;

[2]Nottingham Centre for Geomechanics, University of Nottingham, NG7 2RD, UK;

[3]State Key Laboratory of Simulation and Regulation of Water Cycle in River Basin, China Institute of Water Resources and Hydropower Research, Beijing 100048, P.R. China;

[4] Institute of Mountain Hazards and Environment, CAS, Chengdu 610041, P.R. China.

* Corresponding author: Enlong Liu, Email: liuenlong@scu.edu.cn

Abstract: A coupled elastic-plastic finite element analysis based on simplified consolidation theory for unsaturated soils is used to investigate the coupling processes of water infiltration and deformation of unsaturated soil. By introducing a reduced suction and an elastic-plastic constitutive equation for the soil skeleton, the simplified consolidation theory for unsaturated soils is incorporated into an in-house finite element method code. Using the numerical method proposed here, the generation of pore water pressure and development of deformation can be simulated under evaporation or rainfall infiltration conditions. Through a parametric study and comparison with the test results, the proposed method is found to describe well the characteristics during water evaporation/infiltration into unsaturated soils. Finally, an unsaturated soil slope with water infiltration is analyzed in detail to investigate the development of the displacement and generation of pore water pressure.

Keywords: unsaturated soil, water infiltration, seepage-deformation coupled analysis, finite element method.

Introduction

There are currently many geotechnical engineering problems that are related to unsaturated soils, such as rainfall induced slope failure and expansive soils. For embankment and slope engineering, failures are usually induced by rainfall infiltration because water infiltration will result in an increase in saturation and a change in the distribution of pore-water pressure, which in turn leads to a change in the stress and deformation of a soil. The change of stress and deformation, contrarily, affects the seepage process by modifying the hydraulic properties of porosity and permeability of the soil. Based on these results, it is necessary to conduct a coupled analysis of water infiltration and deformation to study the failure mechanism of unsaturated soil engineering; such a coupled analysis is becoming more important [16].

Many experimental studies have been conducted to investigate the coupling interactions of flow through unsaturated soils with rainfall infiltration. Columns composed of sandy materials have been tested to investigate the leakage as a result of download drainage from an initially saturated state [23], and a new soil column apparatus for laboratory infiltration study was developed that can measure all the variables (pore-water pressures, water contents, inflow rate and outflow rate) instantaneously and automatically in an infiltration process by control of all the boundary conditions [36]. Because more layered soils are encountered than uniform soils in geotechnical engineering, infiltration in layered soils has drawn much attention and has been studied by many researchers [30, 33]. The laboratory test results of vertical infiltration in two soil columns of finer over coarse soils subjected to simulated rainfalls under conditions of no-ponding at the surface and a constant head at the bottom have been presented [37], and an experimental device used to investigate the transient unsaturated-saturated hydraulic response of sand-geotextile layers under conditions of 1-D constant head surface infiltration have been discussed in detail [4]. In addition to laboratory experiments, in-situ tests have been performed to observe the flow through unsaturated soil masses. For example, studies were performed under natural and simulated rainfall on a residual soil slope in Singapore [28] that was instrumented with pore water pressure, water content, and rainfall measuring devices.

Rainfall infiltration into unsaturated soils has also been analyzed by analytical solutions for simple initial and boundary conditions. Ignoring the coupling effects of flow and deformation, Morel-Seytoux [25, 26] obtained an analytical solution by using Green and Ampt's infiltration equation as a basic equation, Basha [2, 3] derived multidimensional non-steady solutions for domains with prescribed surface flux boundary conditions and bottom boundary conditions by using Green's function, and Chen et al. [11] obtained a series solution that has the merit of easy calculation by using a Fourier integral transformation. To improve the understanding of the influence of hydraulic properties and rainfall conditions on rainfall infiltration mechanism and hence on the pore-water pressure distributions in single- and two-layer unsaturated soil systems, an analytical parametric study was performed [38]. Based on Fredlund's incremental-linear elastic constitutive model for unsaturated soil, the analytical solution to a one-dimensional coupled water infiltration and deformation problem by a Fourier integral transform was obtained; the results indicated that the volume change due to a change in soil suction and the ratio of rainfall intensity to saturated permeability has a significant effect on the distribution of the negative pore water pressure and deformations along the soil profile [35]. By assuming that the vertical loading varies exponentially with time, an analytical solution to one-dimensional consolidation in unsaturated soils with a finite thickness under confinement in the lateral direction was also presented [29].

Recently, to address complicated initial and boundary conditions, numerical solutions have been used to analyze the soil engineering related to unsaturated soils. Using the modified Mohr-Coulomb failure criterion [12], the process of infiltration into a slope due to rainfall and its effect on soil slope behavior were examined using a two-dimensional finite element flow-deformation coupled analysis program. The finite element analysis of transient water flow through unsaturated-saturated soils [10] was used to investigate the effects of the hydraulic characteristics, the initial relative degree of saturation, the methods used to consider boundary conditions, and the rainfall intensity and duration on the water pressure in the slopes. The elasto-plastic finite element model [18] in conjunction with a novel analytical formulation for the suction stress above the water table were used to analyze the unsaturated slope stability. A seepage–deformation coupled approach [15] including the effective pore-pressure and the effective stress concept was used to analyze the deformation and the localization of strains on unsaturated soils due to seepage flow. The net stress concept [1] was used to compute the deformations and the variation of the safety factor with time of an unstable slope in a profile of weathered overconsolidated clay using an unsaturated coupled hydromechanical model. Based on the theory of porous media [17], a multiphase coupled elasto-viscoplastic finite-element analysis formulation was used to describe the rainfall infiltration process into a one-dimensional soil column, which demonstrates that the generation of pore water pressure and volumetric strain is mainly controlled by material parameters that describe the soil–water characteristic curve. Based on the existing hydro-mechanical model for non-expansive unsaturated soil, an elastoplastic constitutive model was developed for predicting the hydraulic and mechanical behavior of unsaturated expansive soils [34]. To consider the spatial variability of the properties of the materials of the soil deposits, a stochastic finite element model of unsaturated seepage through a flood defense embankment with randomly heterogeneous material was presented [22]. The stochastic finite element model was also used to simulate the contaminant transport through soils, focusing on the incorporation of the effects of soil heterogeneity [27]. Recently, Borja et al. proposed a physical-based hydro-mechanical continuum model and employed a finite element method to study the series of properties of unsaturated soils, which included the following: (i) the stresses, pore pressures, and deformation within a slope were generated, and then the factor of safety was determined with a limit-equilibrium solution [6]; (ii) the 3-D multi-physical aspects triggering landslides were quantified by accounting for the loss of sediment strength due to increased saturation as well as the frictional drag exerted by the moving fluid [7]; (iii) the effect of the spatially varying degree of saturation on triggering a shear band in granular materials was investigated with new variational formulations for porous solids and two critical state formulations [8]; and (iv) a mathematical framework for a coupled solid-deformation/fluid-diffusion model in unsaturated porous material considering geometric nonlinearity in the solid matrix was developed that relies on the continuum principle of thermodynamics to identify an effective or constitutive stress for the solid matrix, along with a water-retention law that highlights the interdependence of the degree of saturation, suction, and porosity of the material [32].

From the relevant works mentioned above, we know that the coupling processes of water infiltration and deformation of unsaturated soils is an interesting topic that has not yet been fully studied. Solving the problems of unsaturated soil engineering requires slightly simplifying the general consolidation theory for unsaturated soil, which has so many unknowns [13, 20] and has been implemented using numerical methods by only a few researchers. By introducing reduced suction and an elastic-plastic constitutive equation for the soil skeleton, a coupled elastic-plastic finite element analysis based on simplified consolidation theory for unsaturated soils [14, 31], compared with the general or standard consolidation theory for unsaturated soils, is used here to investigate the coupled processes of water infiltration and deformation of unsaturated soil. The generation of pore water pressure and deformation is simulated under rainfall infiltration conditions and then compared with the experimental results, which enables the detailed analysis of an unsaturated soil slope with water infiltration to investigate the development of displacement and generation of pore water pressure.

Simplified consolidation theory for unsaturated soils

Effective stress

The formulation is based firmly within the context of Terzaghi's classical effective stress theory as modified for unsaturated soils by Bishop [5] in the form:

$$\sigma' = \sigma - u_a + \chi(u_a - u_w), \tag{1}$$

in which σ' and σ are the effective and total stress, respectively, u_a is the air pressure in the voids, and u_w is the pore water pressure within the unsaturated soil matrix. The term $s = (u_a - u_w)$ is called the matrix suction. We define the reduced suction $\bar{s}$ by the following expression [31]:

$$\bar{s} = \chi(u_a - u_w). \tag{2}$$

So we have $\chi = \bar{s} / s$, called the coefficient of reduced suction. As shown in Fig. 1, the reduced suction can be determined by comparing the results of the compression curve of saturated soils with those of the drying shrinkage curve of the unsaturated soils. Assuming p and s are the pressure sustained by saturated soils and matrix suction induced in the unsaturated soils with the same void ratio, respectively, we have $\bar{s} = p$ by the equivalent strain theory, so the coefficient of reduced suction can be described by the expression: $\chi = p / s$. Under the general stress state, the coefficient of reduced suction χ is a function of the suction s. When the suction is smaller than the air entry value s_b, the coefficient of reduced suction is equal to unity; when suction is smaller than the air entry value s_b, the coefficient of reduced suction varies with the matrix suction in the manner proposed here as follows:

$$\chi = \left(\frac{s}{s_b}\right)^{-m_2}, \tag{3}$$

in which $s_b = (u_a - u_w)_b$ and m_2 is a materials constant.

Pore air pressure

To signify the air content (air mass) in the voids of a soil element within a unit volume, we define the ratio of the pore air of a unit soil element, n_a, as follows (see appendix I):

$$n_a = [1 - (1 - c_h)S_r]n, \tag{4}$$

in which n is the porosity, c_h is the Henry coefficient of solubility and S_r is the degree of saturation of the soil element. Based on Boyle's law, the density of air in the void ρ_a can be obtained:

$$\rho_a = \rho_{a0}(1 + u_a / p_a), \tag{5}$$

in which, ρ_{a0} is the initial density of air in the void, u_a is the excess air pressure above the reference datum p_a, which is the atmospheric pressure that is equal to 1.01×10^5Pa, and $u_a + p_a$ is the absolute air pressure. Under the conditions that the air in the voids cannot be discharged, we have (see Appendix II):

$$u_a = (\frac{n_{a0}}{n_a} - 1)\, p_a, \tag{6}$$

in which, $n_{a0} = [1-(1-c_h)S_{r0}]n_0$, S_{r0} is the initial degree of saturation, and n_0 is the initial porosity.

If the pore air within the soil element can be discharged freely (that is, the excess pore air could be completely discharged), the pore air pressure generated will finally dissipate and is equal to the atmospheric pressure ($u_a = 0$). By Boyle's law, because the pore air pressure remains constant, the density of the pore air will remain constant. Under these conditions, to dissipate the pore air pressure completely, the change of the volume of the pore air within a unit soil element per unit time is Δn_a, so the mass of the pore air discharged within a unit soil element per unit time is $\rho_a \Delta n_a$.

Under the conditions that the air in the voids is discharged partially, it is assumed that the mass of air discharged per unit time is Δq_a, so we define the discharge speed of pore air, ξ, which is the ratio of the mass of the pore air under discharged partially per unit time to that of the pore air discharged completely per unit time, as follows:

$$\xi = \frac{\Delta q_a}{\rho_a \Delta n_a}. \tag{7}$$

So we can obtain the expression of the increment of pore-air pressure as follows (see Appendix III):

$$\Delta u_a = -\frac{p_a + u_a}{n_a}(1-\xi)\Delta n_a. \tag{8}$$

If ξ is constant, by integrating equation (8), we obtain the expression of u_a as follows (see Appendix IV):

$$u_a = [(\frac{n_{a0}}{n_a})^{(1-\xi)} - 1]\, p_a. \tag{9}$$

When ξ is equal to 0, the equation (9) can be reduced to equation (6); when ξ is equal to 1, $u_a = 0$, which corresponds to the conditions that the air is discharged completely.

Governing equations

Ignoring the flow of dissolved air in the pore-water, the vapor in the pore-air and the influence of temperature, the consolidation equations for unsaturated soils have the following expressions [31]:

① Equilibrium equations in incremental form

$$[L]\{d\sigma\}+\{db\}=0,$$

(10)

② Continuous equations of pore-water

$$\frac{\partial}{\partial t}(S_r n)=\mathrm{div}\left[k_w \,\mathrm{grad}\left(\frac{u_w}{\rho_w g}+z\right)\right],$$

(11)

③ Continuous equations of pore-air

$$\frac{\partial}{\partial t}\left[\rho_a(1-S_r)n+\rho_a c_h S_r n\right]=\mathrm{div}\left[\rho_a k_a \,\mathrm{grad}\left(\frac{u_a}{g}\right)\right],$$

(12)

④ The relationship of the effective stress-displacement

$$\{d\sigma'\}=[D][L]^T\{dU\},$$

(13)

⑤ The relationship of the saturation-matrix suction

$$S_r = f_r(s), \tag{14}$$

⑥ The coefficient of permeability of the pore-water

$$k_w = f_w(s), \tag{15}$$

⑦ The coefficient of permeability of the pore-air

$$k_a = f_a(s), \tag{16}$$

in which,

$$[L]=\begin{bmatrix} \frac{\partial}{\partial x} & 0 & 0 & \frac{\partial}{\partial y} & 0 & \frac{\partial}{\partial z} \\ 0 & \frac{\partial}{\partial y} & 0 & \frac{\partial}{\partial x} & \frac{\partial}{\partial z} & 0 \\ 0 & 0 & \frac{\partial}{\partial z} & 0 & \frac{\partial}{\partial y} & \frac{\partial}{\partial x} \end{bmatrix}$$

, $\{d\sigma\}$ and $\{d\sigma'\}$ are the increments of the total stress and the effective stress, respectively, $\{db\}$ is the increment of the body force, g is the gravitational acceleration, [D] is the matrix of stress-strain and $\{dU\}$ is the increment of displacement.

Simplified equations in 2-Dimensions

In this manuscript, we use equation (9) to describe the change of pore air pressure upon loading, so equation (16) will not be used and the displacements and pore water pressure are solved simultaneously.

From equation (4), we have $\Delta n_a = \frac{\partial n_a}{\partial S_r}\frac{\partial S_r}{\partial s}(\Delta u_a - \Delta u_w) - \frac{\partial n_a}{\partial n}\Delta\varepsilon_v$ and $\Delta\varepsilon_v = -\Delta n$ for a soil element, so the increment of total stress from equation (1) can be described as follows:

$$\Delta\sigma = \Delta\sigma' + A_1\Delta u_w + A_2\Delta\varepsilon_v, \tag{17}$$

in which $A_1 = \dfrac{\chi + s\dfrac{\partial\chi}{\partial s} + P\dfrac{\partial n_a}{\partial S_r}\dfrac{\partial S_r}{\partial s}}{1 + P\dfrac{\partial n_a}{\partial S_r}\dfrac{\partial S_r}{\partial s}}$, $A_2 = \dfrac{(\chi + s\dfrac{\partial\chi}{\partial s} - 1)P\dfrac{\partial n_a}{\partial n}}{1 + P\dfrac{\partial n_a}{\partial S_r}\dfrac{\partial S_r}{\partial s}}$, $P = (1-\xi)(p_a + u_a)/n_a$, $\partial n_a/\partial S_r = -(1-c_h)n$ and $\partial n_a/\partial n = 1-(1-c_h)S_r$. Substituting the above equations into equations (10), we obtain:

$$\begin{aligned} &(d_{11} + A_2)\frac{\partial^2\Delta u_x}{\partial x^2} + (d_{14} + d_{41})\frac{\partial^2\Delta u_x}{\partial x\partial z} + d_{44}\frac{\partial^2\Delta u_x}{\partial z^2} \\ &+ d_{14}\frac{\partial^2\Delta u_z}{\partial x^2} + (d_{12} + d_{44} + A_2)\frac{\partial^2\Delta u_z}{\partial x\partial z} + d_{42}\frac{\partial^2\Delta u_z}{\partial z^2} - A_1\frac{\partial\Delta u_w}{\partial x} = \Delta F_x, \end{aligned} \tag{18a}$$

$$\begin{aligned} &d_{41}\frac{\partial^2\Delta u_x}{\partial x^2} + (d_{21} + d_{44} + A_2)\frac{\partial^2\Delta u_x}{\partial x\partial z} + d_{24}\frac{\partial^2\Delta u_x}{\partial z^2} \\ &+ d_{44}\frac{\partial^2\Delta u_z}{\partial x^2} + (d_{24} + d_{42})\frac{\partial^2\Delta u_z}{\partial x\partial z} + (d_{22} + A_2)\frac{\partial^2\Delta u_z}{\partial z^2} - A_1\frac{\partial\Delta u_w}{\partial z} = \Delta F_z, \end{aligned} \tag{18b}$$

in which Δu_x and Δu_z are the increments of the horizontal (or x) and vertical (or z) displacements, respectively, d_{11}, d_{12}.... are the elements of the elastic-plastic matrix of stress-strain, ΔF_x and ΔF_z are the increments of loads in the horizontal (or x) and vertical (or z) directions, respectively.

From equation (11), the continuous equation of pore-water can be formulated as follows,

$$\mu n \frac{\partial u_w}{\partial t} = -\frac{\partial k_{wx}}{\partial x}\frac{\partial h}{\partial x} - \frac{\partial k_{wz}}{\partial z}\frac{\partial h}{\partial z} + S_r \frac{\partial \varepsilon_v}{\partial t}, \tag{19}$$

in which, $h = u_w / \rho_w g + z$, k_{wx} and k_{wz} are the coefficients of permeability in the horizontal and vertical directions, respectively, and $\mu = \partial S_r / \partial u_w$.

Constitutive equations for unsaturated soils

Soil-water characteristic curve

The soil-water characteristic curve is divided into two sections according to the values of the matrix suction s and the air entry suction s_b. When the value of matrix suction s is smaller than that of the air entry suction s_b, the soil can be assumed to be quasi-saturated and the degree of saturation of quasi-saturated soil is assumed to be S_{r1} (the value of S_{r1} approaches 1.0, such as 0.96), so the degree of saturation can be expressed as follows using Hilf formulation [19]:

$$S_r = S_{r1} \frac{p_a + (u_w + s_b)}{p_a + (1 - c_h) S_{r1} (u_w + s_b)} \qquad (s \le s_b), \tag{20a}$$

in which S_{r1} is the degree of saturation of soil masses when the matrix suction is equal to the value of air entry suction s_b. When the value of matrix suction s is greater than that of the air entry suction s_b, the degree of saturation S_r is computed as follows [9]:

$$S_r = S_{ro} + (S_{r1} - S_{ro})\left(\frac{s}{s_b}\right)^{-m_1} \qquad (s > s_b), \tag{20b}$$

in which S_{r0} and m_1 are soil constants. During the process of drying shrinkage or absorbing water, the parameters S_{r0}, S_{r1} and s_b may be different. By the derivation of equation (20b), we have:

$$\mu = (S_{r1} - S_{ro}) \frac{m_1}{s} \left(\frac{s}{s_b}\right)^{-m_1}. \tag{21}$$

The effect of the degree of saturation on the permeability of unsaturated soils is assumed as follows:

$$k_w = k_{ws} \exp(-c_k \frac{s - s_b}{p_a}), \tag{22}$$

where k_{ws} is the permeability for water under saturated conditions and c_k is constant. When $s \le s_b$, $k_w = k_{ws}$.

Elastic-plastic model for soil skeleton

According to the principle of effective stress, i.e., equation (1), the stress in the following equations of this section refers to the effective stress. Ignoring the influence of temperature, the double hardening elastic-plastic model for saturated soils [24] is used to describe the mechanical features of the soil skeleton of unsaturated soils.

Let $\sigma_m = \frac{1}{3}\sigma_{kk}$, $\sigma_s = \sqrt{\frac{3}{2} s_{ij} s_{ij}}$, $s_{ij} = \sigma_{ij} - \sigma_{kk}\delta_{ij}$, $\varepsilon_s = \sqrt{\frac{2}{3} e_{ij} e_{ij}}$, $e_{ij} = \varepsilon_{ij} - \frac{1}{3}\varepsilon_{kk}\delta_{ij}$. The yield function of the model is expressed as follows:

$$F(\sigma, \varepsilon_v^p, \varepsilon_s^p) = \frac{\sigma_m}{1 - [\frac{\eta}{\alpha(\varepsilon_s^p)}]^m} - p(\varepsilon_v^p), \tag{23}$$

in which, $\eta = \sigma_s / \sigma_m$, and m is the parameter of yield function. When m = 1.2, the shape of the yield surface is close to an ellipse, as shown in Fig. 2. p and α are the two hardening parameters, which can be expressed as the functions of plastic volumetric strain ε_v^p and plastic shear strain ε_s^p, respectively, as follows,

$$p = p_0 \exp(\frac{\varepsilon_v^p}{c_c - c_e}), \tag{24}$$

and

$$\alpha = \alpha_m - (\alpha_m - \alpha_0)\exp(\frac{\varepsilon_s^p}{c_a}), \tag{25}$$

in which, $\varepsilon_v^p = \varepsilon_{kk}^p$, $\varepsilon_s^p = \sqrt{\frac{2}{3} e_{ij}^p e_{ij}^p}$, $e_{ij}^p = \varepsilon_{ij}^p - \frac{1}{3}\varepsilon_{kk}^p \delta_{ij}$, c_c and c_e are the slopes of compressional curve and rebound curve, respectively, and p_0 is the reference pressure with $\varepsilon_v^p = 0$. Equation (24) is in the same form as the hardening parameter of original Cam-clay model. In equation (25),

$\alpha_m = (\sqrt[m]{1+m})\sin\phi$, ϕ is internal frictional angle, and α_0 and c_a are two other parameters that can be determined by unloading triaxial compression test, in which the axial load is kept constant and the confining pressure is reduced gradually.

Assuming that the flow rule is associated, the plastic strain increment can be determined by use of elastic-plastic theory as follows,

$$d\varepsilon_{ij}^{p} = d\lambda \frac{\partial F}{\partial \sigma_{ij}} \qquad (26)$$

Or $$d\varepsilon_{v}^{p} = d\lambda \frac{\partial F}{\partial \sigma_{m}},$$

(27a)

$$d\varepsilon_{s}^{p} = \frac{3}{2} d\lambda \frac{\partial F}{\partial \sigma_{s}},$$

(27b)

where $d\lambda$ is the plastic multiplier, which can be derived from the consistency conditions,

$$\frac{\partial F}{\partial \sigma_{ij}} d\sigma_{ij} + \frac{\partial F}{\partial \varepsilon_{v}^{p}} d\varepsilon_{v}^{p} + \frac{\partial F}{\partial \varepsilon_{s}^{p}} d\varepsilon_{s}^{p} = 0$$

(28)

Substituting for the plastic volumetric strain increment $d\varepsilon_{v}^{p}$ and the plastic shear strain increment $d\varepsilon_{s}^{p}$ in equations (27-a) and (27-b), $d\lambda$ is obtained as follows,

$$d\lambda = \frac{\frac{\partial F}{\partial \sigma_{ij}} d\sigma_{ij}}{H}$$

(29)

in which the Hardening modulus H can be expressed as

$$H = -\frac{3}{2}\frac{\partial F}{\partial \varepsilon_{s}^{p}}\frac{\partial F}{\partial \sigma_{s}} - \frac{\partial F}{\partial \varepsilon_{v}^{p}}\frac{\partial F}{\partial \sigma_{m}} = -\frac{3}{2}\frac{\partial F}{\partial \alpha}\frac{\partial \alpha}{\partial \varepsilon_{s}^{p}}\frac{\partial F}{\partial \sigma_{s}} - \frac{\partial F}{\partial p}\frac{\partial p}{\partial \varepsilon_{v}^{p}}\frac{\partial F}{\partial \sigma_{m}}.$$

(30)

Formulations of the finite-element equations

Analytical solutions to a one-dimensional seepage-deformation coupled problem in unsaturated soil could be derived by considering a homogeneous elastic material. Analytical solutions are simple and easy to implement but cannot account for the complex initial and boundary conditions, the soil heterogeneities [8, 32], the nonlinear stress-strain and the hydraulic relations involved in practical geotechnical problems, whereas the numerical solutions are more practical due to their flexibility. In the following, the formulations of finite element equations for the theory proposed here are presented.

Isoparametric elements are implemented with eight-node interpolating functions for the displacements (u_x, u_z) and four node interpolating functions for the pore water pressures (u_w), which can be expressed as follows,

$$u_x = \sum_{i=1}^{8} N_i u_{xi}, u_z = \sum_{i=1}^{8} N_i u_{zi}, u_w = \sum_{i=1}^{4} \bar{N}_i u_{wi}, \tag{31}$$

in which u_{xi} , u_{zi} and u_{wi} are the nodal variables at nodal point I and N_i and $\bar{N}_i$ are interpolating functions for the displacements and pore-water pressure, respectively. Weak forms of equations (18a), (18b) and (19) are discretized in space and solved by the finite element method [21]. The time domain is divided into a number of elements or steps, and then the integration is performed for each step to obtain the changes of the parameters u_{xi} , u_{zi} and u_{wi} . The step-by-step integrations may then be summed to determine the total change of the parameters. The backward differentiation method is used for the time discretization of the equations (18a), (18b) and (19) as follows:

$$\int_{t_k}^{t_k+\Delta t_k} G dt = \Delta t_k \left[(1-\beta) G_{t_k} + \beta \cdot G_{t_k+\Delta t_k} \right] = \Delta t_k \left[G_{t_k} + \beta \Delta G \right] \tag{32}$$

where Δt_k is the time increment, G_{t_k} and $G_{t_k+\Delta t_k}$ are the corresponding function values at steps t_k and $t_k+\Delta t_k$, respectively, and ΔG is the incremental function value and β is an integral parameter. When $\beta > 0.5$, the difference format is unconditionally stable, and thus, $\beta = 2/3$ is used here.

Therefore, the finite element equations for node i (i = 1, 2, …, N_t) can be formulated as follows,

$$\sum_{j-1}^{N_t} [k_{ij}^{11} \Delta u_{xj} + k_{ij}^{12} \Delta u_{zj} + k_{ij}^{13} \Delta h_j] = \Delta F_{xi}, \tag{33a}$$

$$\sum_{j=1}^{N_t} [k_{ij}^{21} \Delta u_{xj} + k_{ij}^{22} \Delta u_{zj} + k_{ij}^{23} \Delta h_j] = \Delta F_{zi}, \tag{33b}$$

and

$$\sum_{j=1}^{N_t}[k_{ij}^{31}\Delta u_{xj}+k_{ij}^{32}\Delta u_{zj}+k_{ij}^{33}(h_{j0}+\beta\Delta h_j)+s_{ij}\Delta h_j]=\Delta Q_i\,, \qquad (33c)$$

in which N_t is the total number of nodal points; $\Delta F_{xi}, \Delta F_{zi}$ and ΔQ_i are the load increments and flux increment at node i, respectively; h_{i0} and Δh_i are the initial value of the water head and the increment of the water head at node i in a computational time step Δt_k ; $h_i=z_i + u_{wi}/\gamma_w$, in which, z_i is the location of the water head at node i; and γ_w is the weight of water. The elements of the coefficient matrix in the finite element equations (33) are given in the Appendix V.

Numerical simulations

Simulation of the experimental results

The proposed benchmark is based on an experiment performed by Liakopolos [23] on a column of Del Monte sand and instrumented to measure the moisture tension at several points along the column during its desaturation due to gravitational effects. Before the start of the experiment, water was continuously added from the top and allowed to drain freely at the bottom through a filter until the uniform flow conditions were established. At the start of the experiment, the water supply ceased, and the tensiometer readings were recorded, as well as the outflow and outflow rate at the bottom. The test diagram is shown in Fig. 3(a). The initial conditions are as follows: for t=0, s=0 for all the nodes, which corresponds to a steady flow of water through the sand column. Furthermore, a state of mechanical equilibrium is assumed for t=0. All the displacements are related to these initial displacements, which correspond to the equilibrium state. The boundary conditions are as follows.

For the lateral surface: there is no flow horizontally, and $q_w=0$ and $u_x=0$. For the top surface: t>0 and $u_a=p_a$. For the bottom surface: t>0, free water outflow, $u_a=p_a$, s=0 for t>0, $u_x= u_z=0$.

The computed parameters used here are as follows: ρ=2.0 g/cm^3, k_o=0.6, ν=0.3077, n_o=0.2975, k_{ws}=0.03 cm/s, c_k=1.0, c_c=0.006, c_e=0.0001, S_{ro}=0.1, S_{r1}=0.96, m_1= m_2=0.1, s_b=25 kPa, α_m=1.0, α_o=0.75, c_α=0.05 and ξ=0.6. Fig. 3(b) presents the simulated results and the tested results of the development of the pore water pressure at different depths. Compared with the test results and the simulated results proposed previously, the new method proposed here can model the drying shrinkage process of unsaturated soils.

Parametric study

(a) Effects of discharge speed of pore air ξ

The mesh, shown in Figure 4(a), is used to simulate seepage-deformation processes under infiltration conditions in only the vertical direction (z direction) with different discharge speeds of the pore air ξ. The soil mass is 100 cm in length and 10 cm in width, with infiltration through the upper surface. The initial suction distribution is shown in Fig. 4(b). The boundary conditions are as follows.

For the lateral surface: there is no flow horizontally, and $q_w=0$ and $u_x=0$. For the top surface: drained freely (water and air). For the bottom surface: s=0 (water level located at the bottom surface) for t>0 and $u_x= u_z=0$.

The soil mass is infiltrated by rainfall with rate of 0.576 mm/hours, and the computed parameters employed are as follows: ρ=2.0 g/cm^3, k_o=0.6, ν=0.3077, n_o=0.432, k_{ws}=0.000088 cm/s, c_k=1.0, c_c=0.06, c_e=0.01, S_{ro}=0.2, S_{r1}=0.998, $m_1= m_2$=0.1, s_b=25kPa, α_m=1.0, α_o=0.75 and c_α=0.05. The discharge speeds of pore air ξ are assumed to be 0.2, 0.4, 0.6, 0.8 and 1.0, respectively.

Fig. 4 (c)-(e) show the variation of suction during rainfall infiltration with different discharge speed of pore air ξ. It is obvious that the discharge speed of pore air has a greater influence on the development of suction in the unsaturated soils. In the process of infiltration, the magnitude of the suction with smaller ξ is greater than that of the suction with larger ξ because the pore air pressure will decrease with the increasing value of ξ. With rainfall infiltration, the magnitude of the suction becomes smaller for the same value of ξ.

(b) Effects of the evaporation intensity I

The effects of evaporation intensity I on the seepage-deformation coupling processes of unsaturated soils are investigated using the computational mesh and boundary conditions shown in Fig. 5 (a) with different values of evaporation intensity I. Before the start of the evaporation, the soils are fully saturated. The initial conditions are as follows: for t=0, s=0 for all the nodes, which corresponds to a steady flow of water through the soil column. Furthermore, a state of mechanical equilibrium is assumed for t=0. All the displacements are related to these initial displacements, which correspond to the equilibrium state. The boundary conditions are as follows: For the lateral surface: there is no flow horizontally, and $q_w=0$ and $u_x=0$. For the top surface: evaporation, t>0, $u_a=p_a$ and a drained boundary (water and air). For the bottom surface: $u_a=p_a$, s=0 for t>0, and $u_x= u_z=0$. The computed parameters used here are as follows: ρ=2.0 g/cm^3, k_o=0.6, ν=0.3077, n_o=0.2975, k_{ws}=0.003 cm/s, c_k=1.0, c_c=0.006, c_e=0.0001, S_{ro}=0.1, S_{r1}=0.96, m_1= m_2=0.1, s_b=25kPa, α_m=1.0, α_o=0.75 and c_α=0.05, ξ=0.6. The evaporation intensity I = 0.012 cm/hrs, 0.024 cm/hrs and 0.036 cm/hrs are used here to study the influence of evaporation intensity on the features of the soil column.

Fig. 5 (b)-(d) present the distributions of the pore water pressure during the process of evaporation with different values of evaporation intensity, which demonstrates that the magnitude of the evaporation intensity has great influence on the development of pore water pressure in the unsaturated soils. During the process of evaporation, the magnitude of the pore water pressure (compressive is positive) increases gradually with the same depth at the same time. With the increase of the evaporation intensity, the magnitude of the pore water pressure also increases gradually at the same time with the same depth of the soil column. When the magnitude of the evaporation intensity is greater on the upper surface of the soil column, there is greater pore water pressure with a negative value, thus resulting in equilibrium of the unsaturated soil masses.

(c) Effects of the saturated permeability k_{ws}

For the computational mesh and boundary conditions shown in Fig. 5(a), the effects of the permeability of unsaturated soils k_{ws} on the seepage-deformation coupling processes of unsaturated soils are investigated with different values of k_{ws}. The initial and boundary conditions are the same as those of section (b) discussed above. The computed parameters used here are as follows: ρ=2.0 g/cm^3, k_o=0.6, ν=0.3077, n_o=0.2975, I=0.012 cm/hrs, c_k=1.0, c_c=0.006, c_e=0.0001, S_{ro}=0.1, S_{r1}=0.96, m_1= m_2=0.1, s_b=25kPa, α_m=1.0, α_o=0.75, c_α=0.05, and ξ=0.6. The saturated permeability k_{ws}=0.03 cm/s, 0.003 cm/s and 0.0008 cm/s are used here to investigate the influence of the saturated permeability on the features of the soil column.

Figs. 6 (a)-(c) present the distributions of the pore water pressure during the process of evaporation with different values of saturated permeability, which also demonstrates that the magnitude of the saturated permeability affects the development of pore water pressure in the unsaturated soils greatly. With the decrease of the saturated permeability, the magnitude of the pore water pressure increases gradually at the same time with the same depth of the soil column. In addition, the magnitude of pore water pressure increases gradually with the same depth at the same time for the same saturated permeability. The greater the saturated permeability is, the quicker the dissipation of pore water. Thus, we obtained the computational results presented here.

Simulation of the unsaturated soil slope with rainfall infiltration

The seepage-deformation processes under evaporation and rainfall infiltration conditions are simulated for an unsaturated soil slope that is 20 m in depth and 54 m in width. The computational mesh and boundary conditions are shown in Figure 7(a).

For the lateral surfaces, there are undrained and constrained boundaries ($u_x = u_z = 0$); for the bottom surface, a constrained boundary, the pore water pressure is zero all the time with the surface of the water table; for the upper surfaces composed of three planes, they drain freely, and evaporation/infiltration occurs on these surfaces. When t=0, the soil slope is saturated and is in equilibrium with the weight stress state. During the first 1100 days, the evaporation rate of the soil slope is 0.3 mm per day, and during the subsequent 300 days, the infiltration rate of rainfall is 0.5 mm per day. The computed parameters are as follows: ρ=2.0 g/cm^3, k_o=0.6, ν=0.3077, e_o=0.7, k_{ws}=0.000001 cm/s, c_k=0.2, c_c=0.0332, c_e=0.0064, S_{ro}=0.2, S_{r1}=0.96, m_1= m_2=0.1, s_b=20 kPa, α_m=1.0, α_o=0.75, ξ=0.6 and c_α=0.05.

Figs. 7 (b) and (c) present the distribution of the pore water pressure at the end of the evaporation and rainfall infiltration, respectively. At the end of evaporation, the pore water with a negative value is highest near the upper surfaces of the soil slope, and it reduces gradually with the water infiltration into the unsaturated soil slope. Figs. 7 (d) and (e) present the distributions of the displacement at the end of evaporation and rainfall infiltration, respectively. From the simulation of the evaporation and rainfall infiltration for an unsaturated soil slope, the method proposed here can model the seepage-deformation process of unsaturated soils qualitatively.

Conclusions

A new FEM code was developed on the basis of a simplified consolidation theory for unsaturated soils that can be used to analyze the seepage-deformation of unsaturated soil slope under evaporation/rainfall infiltration conditions. The numerical examples demonstrate that the reduced suction and constant discharge speed of the pore air can be introduced to simplify the consolidation equations for unsaturated soils, thereby making it easy to program the consolidation theory into the numerical analysis code of the elastic-plastic finite element method. Through a parameter study and comparison with the tested results, the results of this study demonstrated that the proposed method can describe well the features in the process of water evaporation/infiltration into unsaturated soils.

References

1. Alonso EE, Gens A, Delahaye CH (2003) Influence of rainfall on the deformation and stability of a slope in overconsolidated clays: a case study. Hydrogeology Journal 11: 174-192.
2. Basha HA (1999) Multidimensional linearized non-steady infiltration with prescribed boundary conditions at the soil surface. Water Resources Research 35(1): 75-83.
3. Basha HA (2000) Multidimensional linearized non-steady infiltration toward a shallow water table. Water Resources Research 36(9): 2567-2573.
4. Bathurst RJ, Ho AF, Siemens G (2007) A column apparatus for investigation of 1-D unsaturated-saturated response of sand-geotextile system. Geotechnical Testing Journal 30(6): 1-9.
5. Bishop AW (1955) The principal of effective stress. Teknsik Ukeblad 106: 859-863.
6. Borja RI, Liu X, White JA (2012) Multiphysics hillslope processes triggering landslides. Acta Geotechnica 7:261-269.
7. Borja RI, White JA, Liu X, Wu W (2012) Factor of safety in a partially saturated slope inferred from hydro-mechanical continuum modeling. International Journal for Numerical and Analytical Methods in Geomechanics 36(2): 236-248.
8. Borja RI, Song X, Wu W. (2013). Cam-clay plasticity, Part VII: Triggering a shear band in variably saturated porous media. Comput. Methods Appl. Mech. Engrg 261-262: 66-82.
9. Brooks RH, Corey AT (1964) Hydraulic properties of porous medium. Hydrology Paper No.3, Civil Engineering Department, Colorado State University, Fort Collins, Co.
10. Cai F, Ugai K (2004) Numerical analysis of rainfall effects on slope stability. International Journal of Geomechanics 4(2): 69-78.

11. Chen JM, Tan YC, Chen CH (2001) Multidimensional infiltration with arbitrary surface fluxes. Journal of Irrigation and Drainage Engineering 127(6): 370-377.

12. Cho SE, Lee SR (2001) Instability of unsaturated soil slopes due to infiltration. Computers and Geotechnics 28: 185-208.

13. Conte E (2004) Consolidation analysis for unsaturated soils. Canadian Geotechnical Journal 41: 599-612.

14. Deng G, Shen ZJ (2006) Numerical simulation of crack formation process in clays during drying and wetting. Geomechanics and Geoengineering: An International Journal 1(1): 27-41.

15. Ehlers W, Graf T, Ammann M (2004) Deformation and localization analysis of partially saturated soil. Compute Methods in Applied Mechanics and Engineering 193: 2885-2910.

16. Fredlund DG (2006) Unsaturated soil mechanics in engineering practice. Journal of Geotechnical and Geoenvironmental Engineering 132(3): 286-321.

17. Garcia E, Oka F, Kimoto S (2011) Numerical analysis of a one-dimensional infiltration problem in unsaturated soil by a seepage-deformation coupled method. International Journal for Numerical and Analytical Methods in Geomechanics 35(5): 544-568.

18. Griffiths DV, Lu N (2005) Unsaturated slope stability analysis with steady infiltration or evaporation using elasto-plastic finite elements. International Journal for Numerical and Analytical Methods in Geomechanics 29: 249-267.

19. Hilf JW (1948) Estimating construction pore pressures in rolled earth dams. In Proc.2nd Int.Conf. Soil Mech. Found. Eng. Rotterdam, The Netherlands, vol.3: 234-240.

20. Khalili N, Valliappan S, Wan CF (1999) Consolidation of fissured clays. Geotechnique 49: 75-89.

21. Lewis RW, Schrefler BA (1987).The finite element method in the deformation and consolidation of porous media. Wiley: New York.

22. Le TMH, Gallipoli D, Sánchez M, Wheeler SJ (2012). Stochastic analysis of unsaturated seepage through randomly heterogeneous earth embankments. International Journal of Numerical and Analytical Method in Geomechanics 36:1056-1076.

23. Liakopoulos A (1964). Transient flow through unsaturated porous media. Ph.D. Thesis, University of California at Berkeley.

24. Liu EL, Xing, HL (2009). A double hardening thermo-mechanical constitutive model for overconsolidated clays. Acta Geotechnica 4: 1-6.

25. Morel-Seytoux HJ (1978). Derivation of equations for variable rainfall infiltration. Water Resources Research 14(4): 561-568.

26. Morel-Seytoux HJ (1981) Analytical results for prediction of variable rainfall infiltration. Journal of Hydrology 59: 209-230.

27. Nezhad MM, Javadi AA, Al-Tabbaa A, Abbasi F. (2013). Numerical study of soil heterogeneity effects on contaminant transport in unsaturated soil (model development and validation). International Journal of Numerical and Analytical Method in Geomechanics 37:278-298.

28. Rahardjo H, Lee TT, Leong EC, Rezaur RB (2005) Response of a residual soil slope to rainfall. Canadian Geotechnical Engineering 42: 340-351.

29. Qin A, Sun D, Tan Y (2010) Analytical solution to one-dimensional consolidation in unsaturated soils under loading varying exponentially with time. Computers and Geotechnics 37: 233-238.

30. Serrano SE (1990) Modeling infiltration in hysteretic soils. Advance in Water Resources 13(1): 12-23.

31. Shen ZJ (2003) Simplified consolidation theory for unsaturated soils and its application. Hydro-science and Engineering (4):1-6 (in Chinese with English abstract).

32. Song X, Borja RI (2014). Mathematical framework for unsaturated flow in the finite deformation range. Int. J. Num. Meth. Engng 97:658-682.

33. Stauffer F, Dracos T (1986) Experimental and numerical study of water and solute infiltration in layered porous media. Journal of Hydrologic Engineering 84: 9-34.

34. Sun W, Sun D (2012). Coupled modelling of hydro-mechanical behavior of unsaturated compacted expansive soils. International Journal of Numerical and Analytical Method in Geomechanics 36:1002-1022.

35. Wu LZ, Zhang LM (2009) Analytical solution to 1D coupled water infiltration and deformation in unsaturated soils. International Journal for Numerical and Analytical Methods in Geomechanics 33: 773-790.

36. Yang H, Rahardjo H, Wibawa B, Leong EC (2004) A soil column apparatus for laboratory infiltration study. Geotechnical Testing Journal 27(4): 1-9.

37. Yang H, Rahardjo H, Leong EC (2006) Behavior of unsaturated layered soil columns during infiltration. Journal of Hydrologic Engineering 11(4): 329-337.

38. Zhan LT, Ng CWW(2004) Analytical analysis of rainfall infiltration mechanism in unsaturated soils. International Journal of Geomechanics 4: 273-284.

Appendix I

From the simplified phase diagrams (see Fig. A1) for an unsaturated soil, we have

$$V_v = V_a + V_w, \text{ and } V = V_a + V_w + V_s = 1,$$

$$S_r = V_w/V_v,\ n = V_v/V,$$

so we obtain $V_a=V_v$ - V_w. However, for the unsaturated soils, some air is embedded in the water, which can be formulated by the simplified method as $V'_a=c_hV_w$, so the total air content of a unit volume of unsaturated soil element can be obtained:

$$V_a+V'_a=V_v-V_w+c_hV_w=nV[1-S_r+c_h S_r]=[1-S_r+c_h S_r]\,n.$$

We define $n_a=[1-S_r+c_hS_r]n=[1-(1-c_h)S_r]n$, where n is the ratio of the pore air of a unit soil element, which signifies the air content in the voids of a soil element within unit volume.

Appendix II

For a unit volume soil element, the pore air pressure u_a will be generated upon loading. Under the conditions that the air in the voids cannot be discharged, from Boyle's law, we have

$$(p_a+u_a)(V_a+c_hV_w)=(p_a+u_{a0})(V_{a0}+c_hV_{w0}), \quad \text{(II-1)}$$

in which, p_a is the atmospheric pressure, u_a is the pore air pressure, V_{a0} is the initial content of pore air of a unit volume soil element (the corresponding pore air pressure $u_{a0}=0$), and V_a is the content of pore air of a unit volume soil element. For a unit volume soil element (see Fig. A1), we have $V_w=nS_r$ and $V_a=n(1-S_r)$. Combining equation (4), $n_a=[1-(1-c_h)S_r]n$, and equation (II-1), we have

$$(p_a+u_a)n_a=(p_a+u_{a0})n_{a0}, \quad \text{(II-2)}$$

in which, n_{a0} is the initial ratio of pore air of a unit soil element, $n_{a0}=[1-(1-c_h)S_{r0}]n_0$, S_{r0} is initial degree of saturation and n_0 is initial porosity.

Because the initial air pressure is equal to the atmospheric pressure ($u_{a0}=0$), from equation (II-2), we have:

$$u_a=(\frac{n_{a0}}{n_a}-1)\,p_a. \quad \text{(II-3) or (6)}$$

Appendix III

In the following, we ignore the flow of the dissolved air in the pore-water, the vapor in the pore-air and the influence of temperature. For a unit volume soil element, the mass of pore air discharged per unit time has the following equation (mass conservation equation):

$$\frac{\partial}{\partial t}\left[\rho_a(1-S_r)n+\rho_a c_h S_r n\right]=\frac{\partial}{\partial t}\left[\rho_a n_a\right]=\frac{dq_a}{dt},$$

(III-1)

in which q_a is the mass of pore air discharged within a unit soil element. From equation (III-1), we can deduce the following equation in incremental form:

$$\Delta\rho_a \cdot n_a + \rho_a \cdot \Delta n_a = \Delta q_a. \qquad \text{(III-2)}$$

Differentiating equation (5), $\rho_a = \rho_{a0}(1 + u_a / p_a)$, we have

$$\Delta\rho_a = \rho_{a0} \cdot \Delta u_a / p_a. \qquad \text{(III-3)}$$

From equation (7), we have

$$\Delta q_a = \xi \cdot \rho_a \cdot \Delta n_a, \qquad \text{(III-4)}$$

Substituting equations (III-3) and (III-4) into equation (III-2), we obtain

$$n_a \cdot \rho_{a0} \cdot \Delta u_a / p_a + \rho_a \cdot \Delta n_a = \xi \cdot \rho_a \cdot \Delta n_a, \qquad \text{(III-5)}$$

Substituting equation (5), $\rho_a = \rho_{a0}(1 + u_a / p_a)$, into equation (III-5), we have

$$\Delta u_a = -\frac{p_a + u_a}{n_a}(1 - \xi)\Delta n_a. \qquad \text{(III-6) or (8)}$$

Appendix IV

The equation (8) can be expressed as:

$$\frac{du_a}{p_a + u_a} = -\frac{1 - \xi}{n_a} dn_a, \qquad \text{(IV-1)}$$

Integrating the above equation, we obtain the following:

$$\ln(p_a + u_a) = -(1 - \xi)\ln(n_a) + \text{const.}, \qquad \text{(IV-2)}$$

Substituting the initial conditions n_{a0} and u_{a0} into equation (IV-2), we have

$$\text{const.} = \ln[(p_a + u_{a0}) n_{a0}^{(1-\xi)}], \qquad \text{(IV-3)}$$

Combining equations (IV-2) and (IV-3), we have

$$u_a = [(\frac{n_{a0}}{n_a})^{(1-\xi)} - 1] p_a. \qquad \text{(IV-4)}$$

Appendix V

The elements of the coefficient matrix in the finite element equation (33) are as follows,

$$k_{ij}^{11}=\int[(d_{11}+A_2)\frac{\partial N_i}{\partial x}\frac{\partial N_j}{\partial x}+d_{44}\frac{\partial N_i}{\partial z}\frac{\partial N_j}{\partial z}+d_{14}(\frac{\partial N_i}{\partial x}\frac{\partial N_j}{\partial z}+\frac{\partial N_j}{\partial x}\frac{\partial N_i}{\partial z})]dxdz, \quad \text{(V-1)}$$

$$k_{ij}^{12}=\int[(d_{12}+A_2)\frac{\partial N_i}{\partial x}\frac{\partial N_j}{\partial z}+d_{14}\frac{\partial N_i}{\partial x}\frac{\partial N_j}{\partial x}+d_{24}\frac{\partial N_i}{\partial z}\frac{\partial N_j}{\partial z}+d_{44}\frac{\partial N_j}{\partial x}\frac{\partial N_i}{\partial z}]dxdz, \quad \text{(V-2)}$$

$$k_{ij}^{21}=\int[(d_{12}+A_2)\frac{\partial N_i}{\partial z}\frac{\partial N_j}{\partial x}+d_{14}\frac{\partial N_i}{\partial x}\frac{\partial N_j}{\partial x}+d_{24}\frac{\partial N_i}{\partial z}\frac{\partial N_j}{\partial z}+d_{44}\frac{\partial N_i}{\partial x}\frac{\partial N_j}{\partial z})]dxdz, \quad \text{(V-3)}$$

$$k_{ij}^{22}=\int[(d_{22}+A_2)\frac{\partial N_i}{\partial z}\frac{\partial N_j}{\partial z}+d_{44}\frac{\partial N_i}{\partial x}\frac{\partial N_j}{\partial x}+d_{24}(\frac{\partial N_i}{\partial z}\frac{\partial N_j}{\partial x}+\frac{\partial N_j}{\partial z}\frac{\partial N_i}{\partial x})]dxdz, \quad \text{(V-4)}$$

$$k_{ij}^{33}=-\int[k_x\frac{\partial N_i}{\partial x}\frac{\partial N_j}{\partial x}+k_z\frac{\partial N_i}{\partial z}\frac{\partial N_j}{\partial z}]dxdz, \quad \text{(V-5)}$$

$$k_{ij}^{13}=-\rho_w g\int A_1\frac{\partial \bar{N}_i}{\partial r}\bar{N}_j ddz, \quad \text{(V-6)}$$

$$k_{ij}^{23}=-\rho_w g\int A_1\frac{\partial \bar{N}_i}{\partial z}\bar{N}_j dxdz, \quad \text{(V-7)}$$

$$k_{ij}^{31}=-\rho_w g\int S_r\frac{\partial \bar{N}_j}{\partial x}\bar{N}_i dxdz, \quad \text{(V-8)}$$

$$k_{ij}^{32}=-\rho_w g\int S_r\frac{\partial \bar{N}_j}{\partial z}\bar{N}_i dxdz, \quad \text{(V-9)}$$

$$s_{ij}=-\rho_w g\int c_s N_i N_j dxdz, \quad \text{(V-10)}$$

where $c_s=\mu n/S_r$ 。

List of figures

pore water pressure with evaporation intensity I=0.024 cm/hours. (d) The distribution of pore water pressure with an evaporation intensity I=0.036 cm/hours.

Fig. 6 Effects of saturated permeability k_{ws}. (a) The distribution of pore water pressure with k_{ws}=0.03 cm/s. (b) The distribution of pore water pressure with k_{ws}=0.003 cm/s. (c) The distribution of pore water pressure with k_{ws}=0.0008 cm/s.

Fig. 7 Simulation of unsaturated soil slope with rainfall infiltration. (a) Computational mesh and boundary conditions. (b) Pore water pressure distribution at the end of evaporation (kPa). (c) Pore water pressure distribution at the end of infiltration (kPa). (d) Displacement distribution at the end of evaporation. (e) Displacement distribution at the end of rainfall infiltration.

Fig. A1 Simplified three phase diagram.

Figure

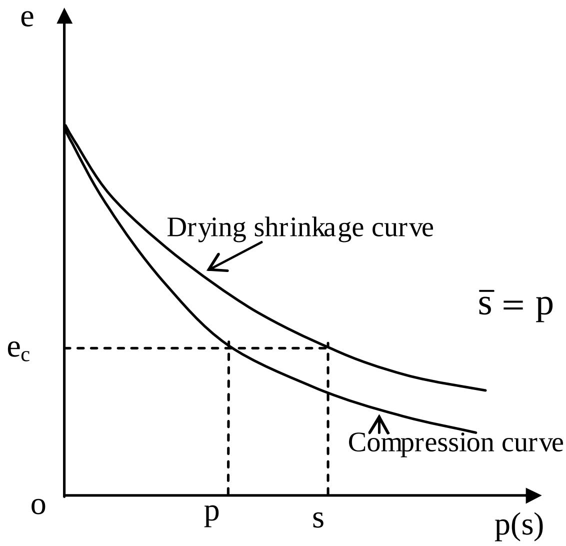

Fig.1 Determination of the reduced suction

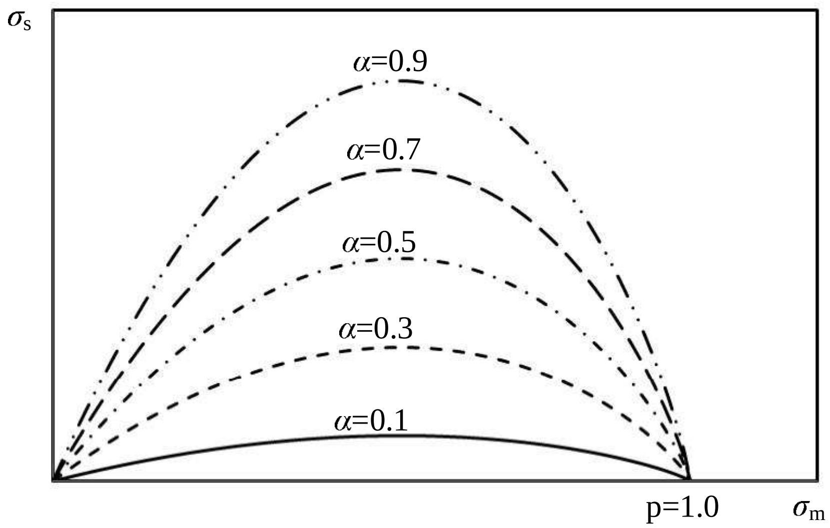

Fig.2 (a) p=const.

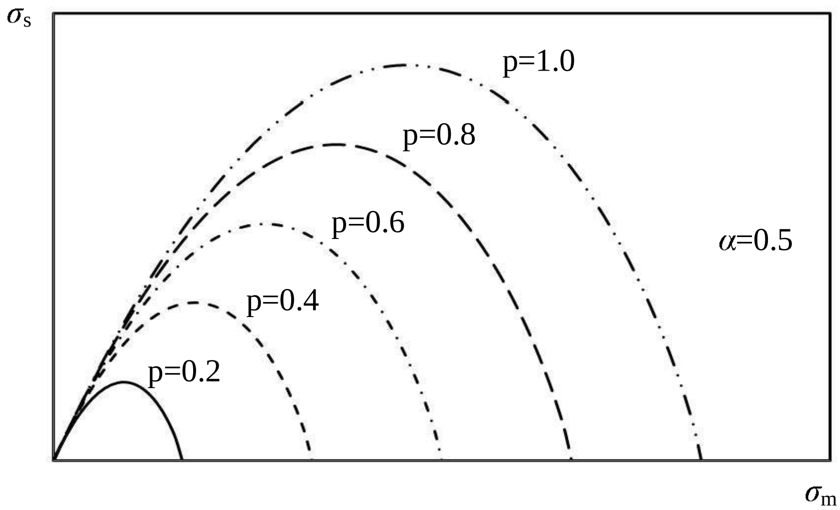

Fig.2 (b) α=const.

Fig.2 Double hardening yield surfaces

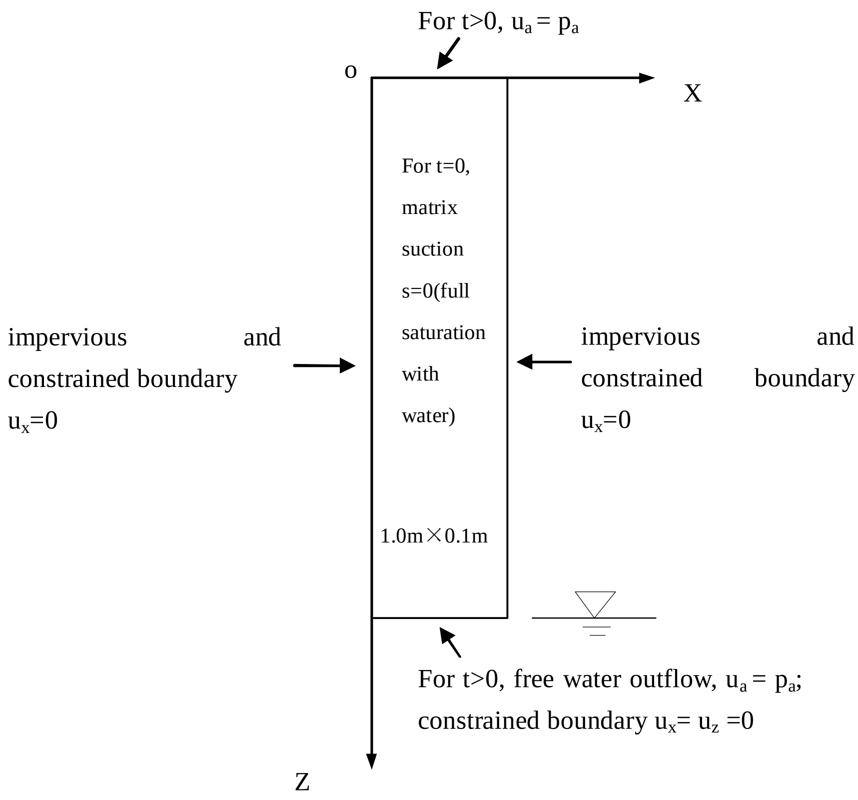

Fig.3 (a)The Liakopoulos test problem

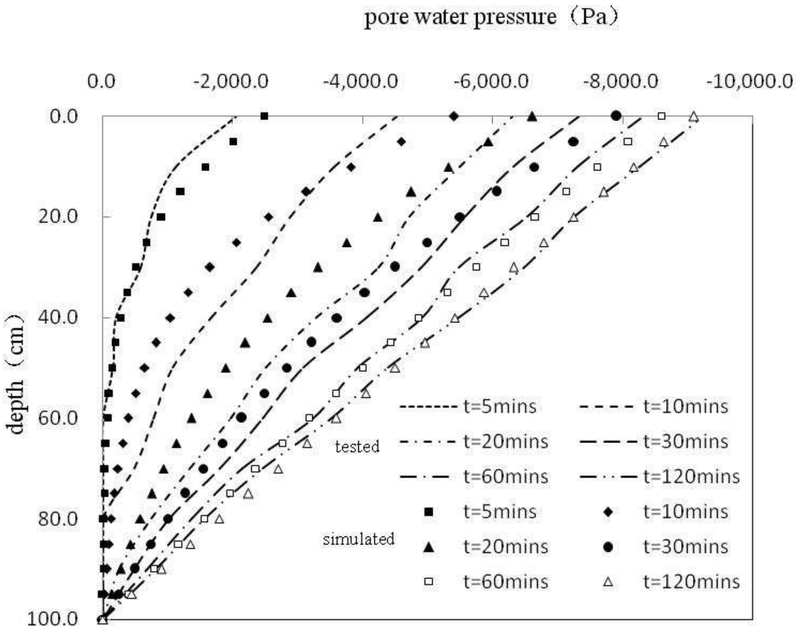

Fig.3 (b) Comparisons with laboratory test results of the Liakopoulos test problem (Liakopolos 1965)

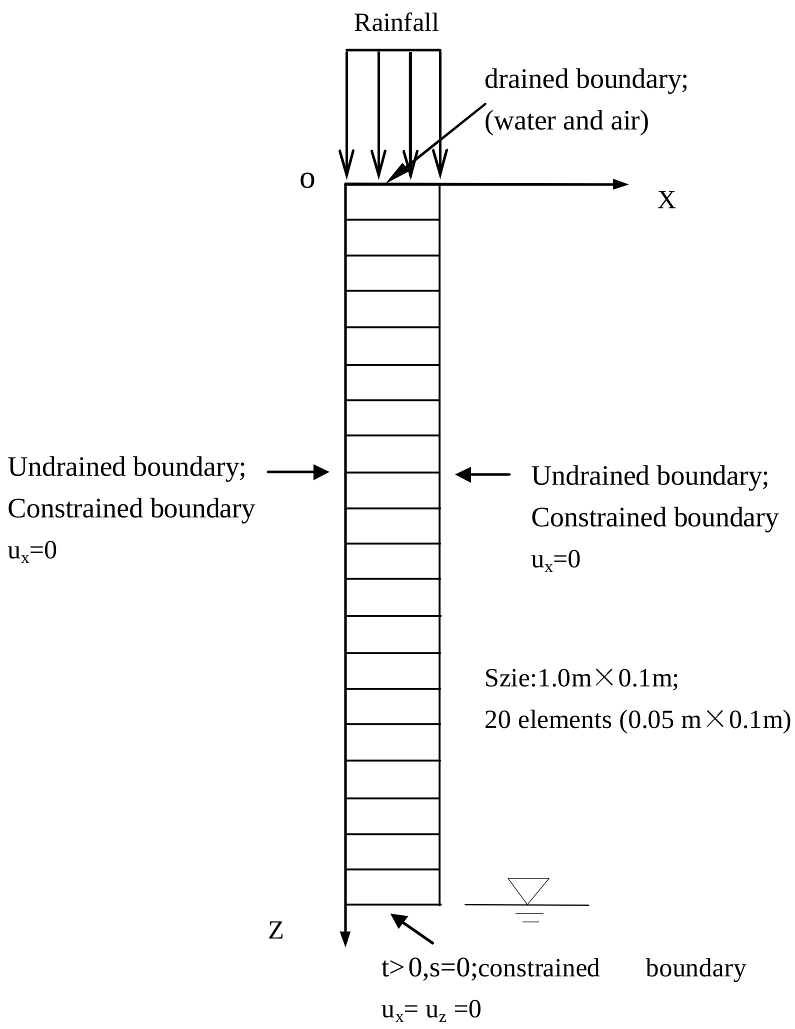

Fig.4(a). Computational mesh and boundary conditions

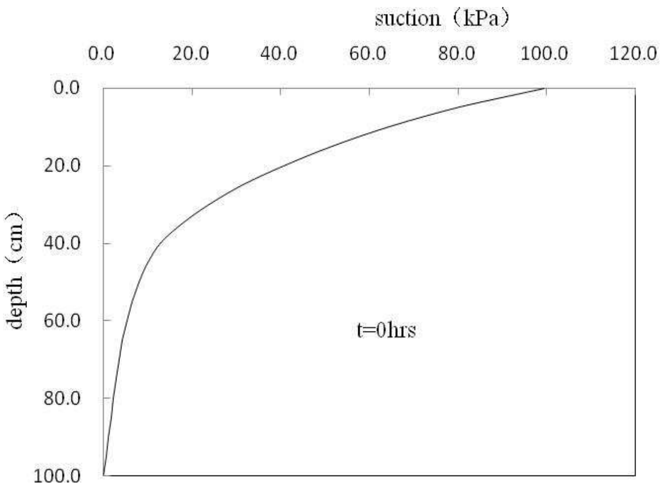

Fig.4(b). The initial suction distribution at t=0.0hours

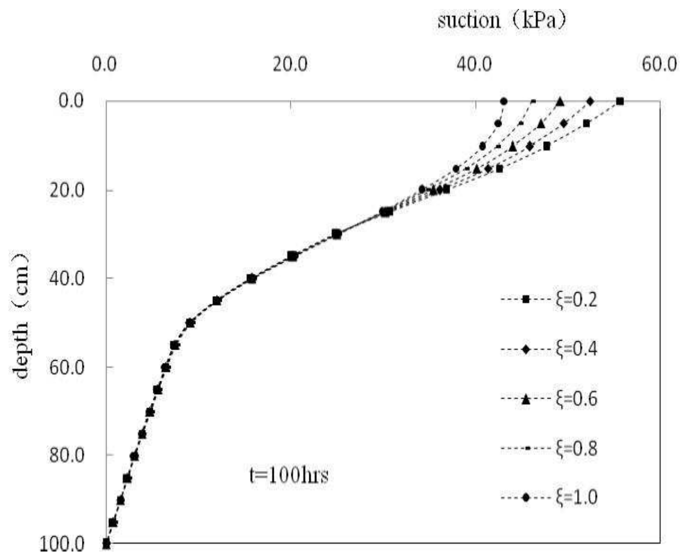

Fig.4(c). The suction distribution at t=100hours of infiltration

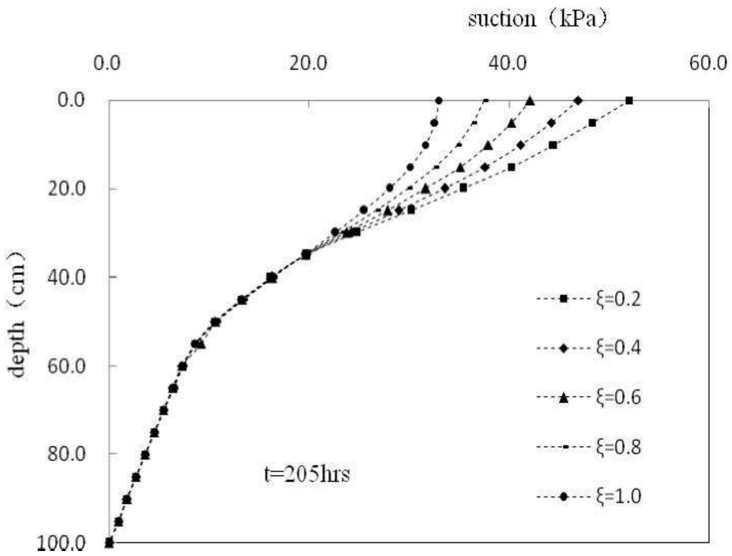

Fig.4(d). The suction distribution at t=205hours of infiltration

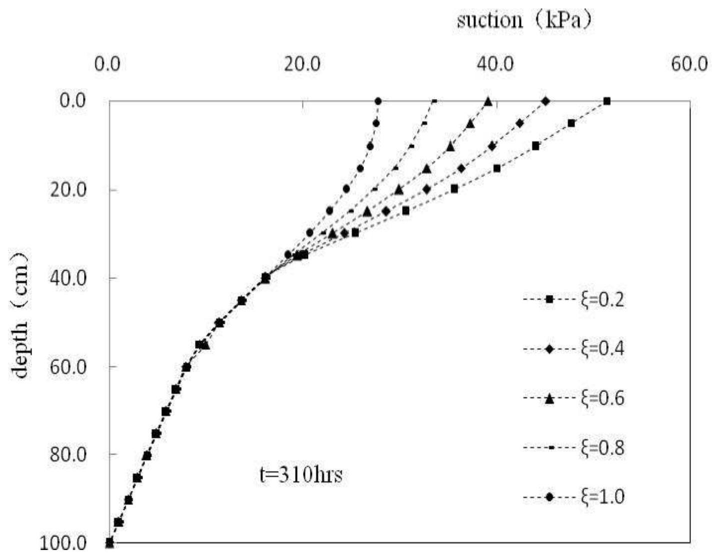

Fig.4(e). The suction distribution at t=310hours of infiltration

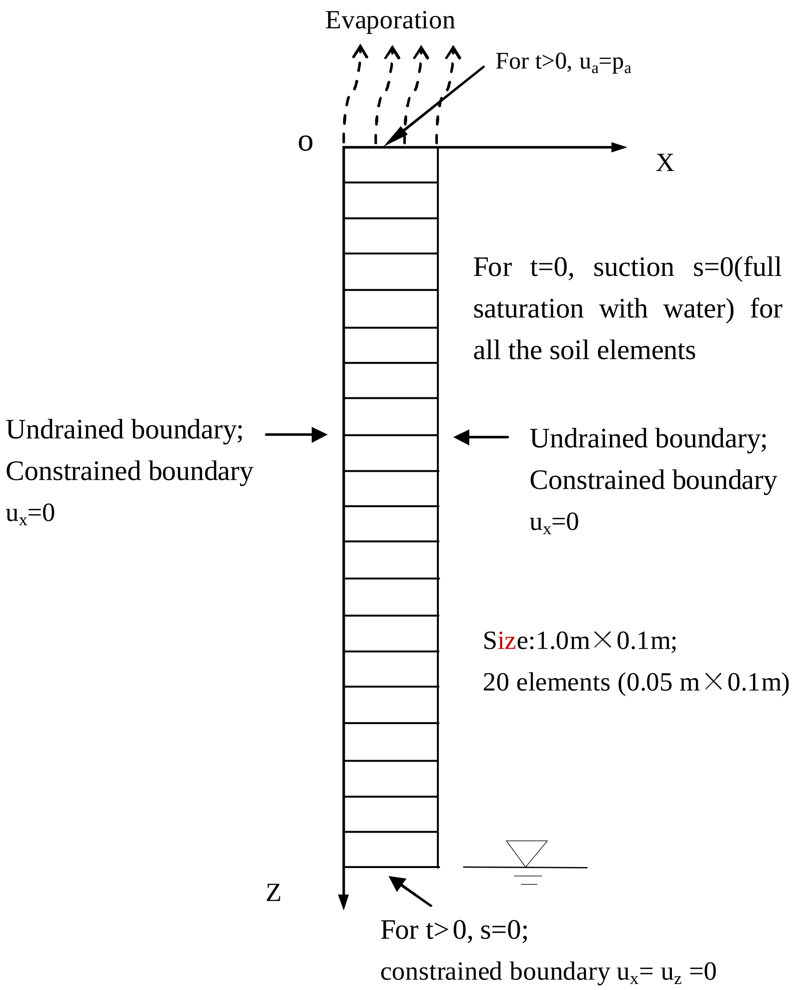

Fig.5(a). Computational mesh and boundary conditions

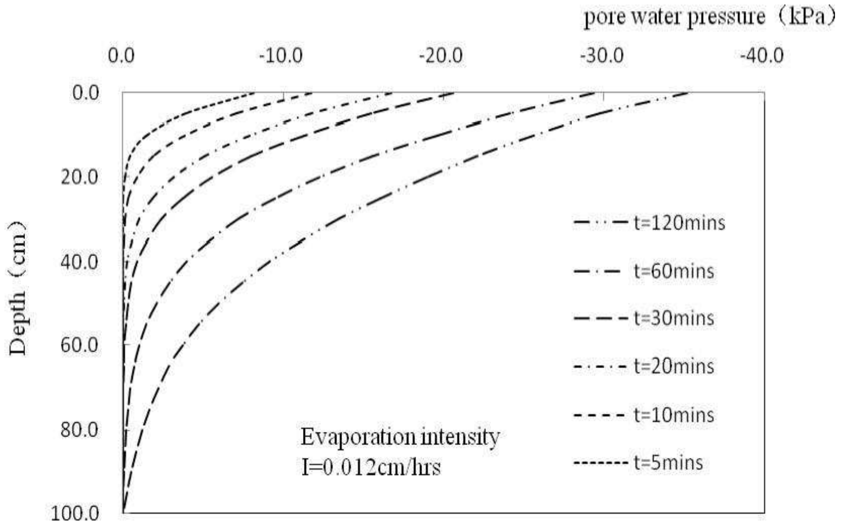

Fig.5(b). The distribution of pore water pressure with evaporation intensity I=0.012cm/hours

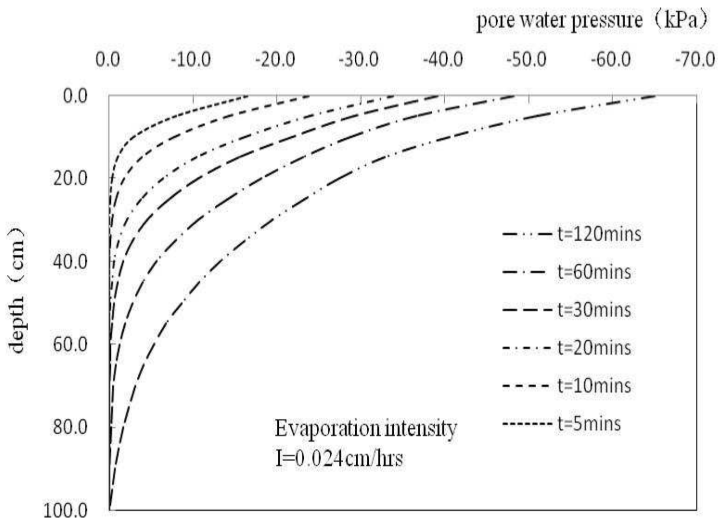

Fig.5(c). The distribution of pore water pressure with evaporation intensity I=0.024cm/hours

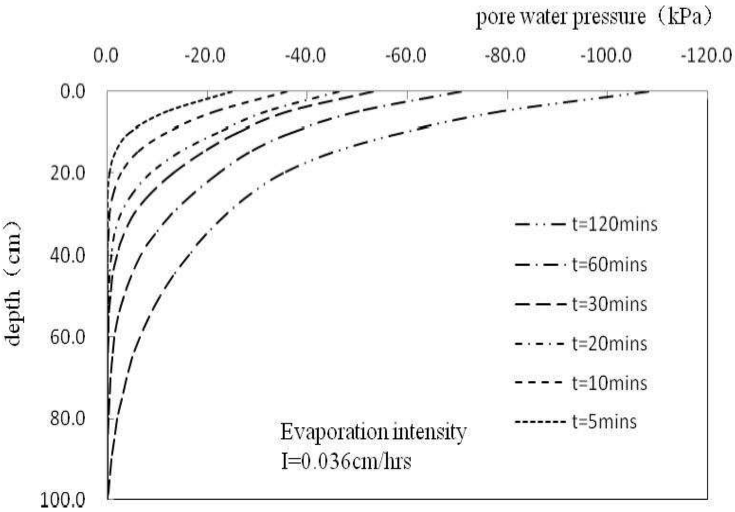

Fig.5(d). The distribution of pore water pressure with evaporation intensity I=0.036cm/hours

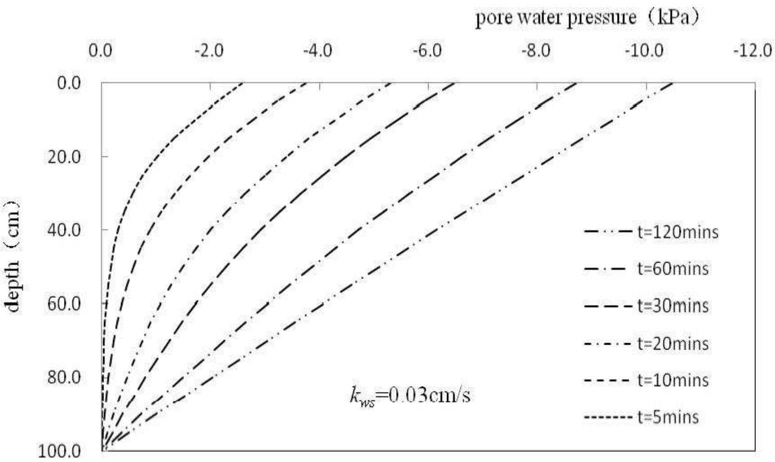

Fig.6(a). The distribution of pore water pressure with k_{ws}=0.03cm/s

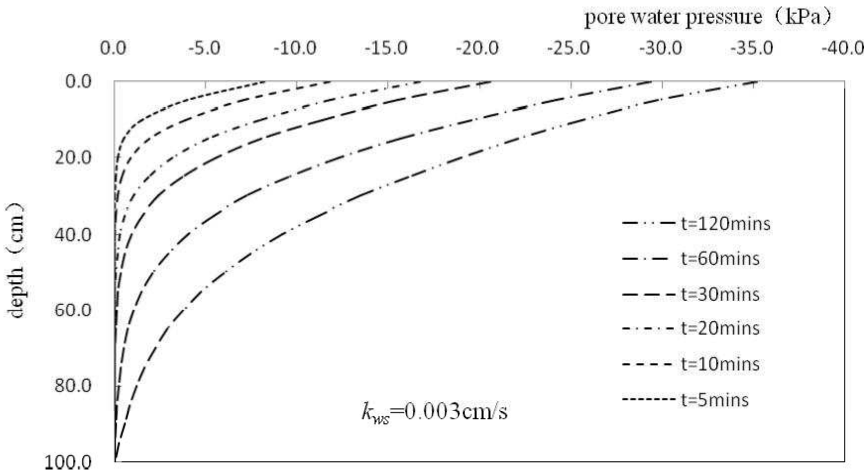

Fig.6(b). The distribution of pore water pressure with k_{ws}=0.003cm/s

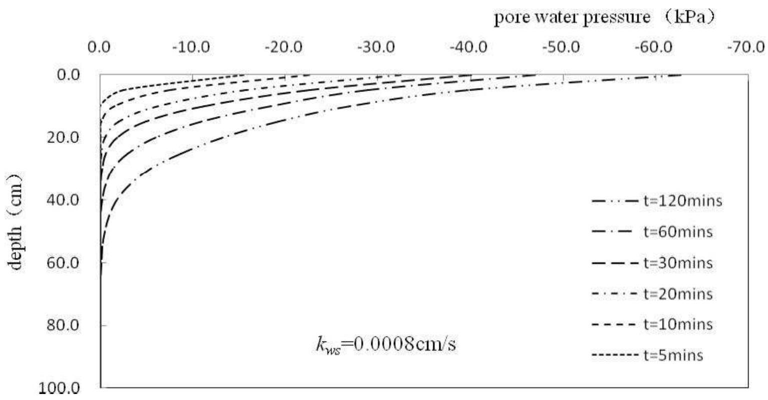

Fig.6(c). The distribution of pore water pressure with k_{ws}=0.0008cm/s

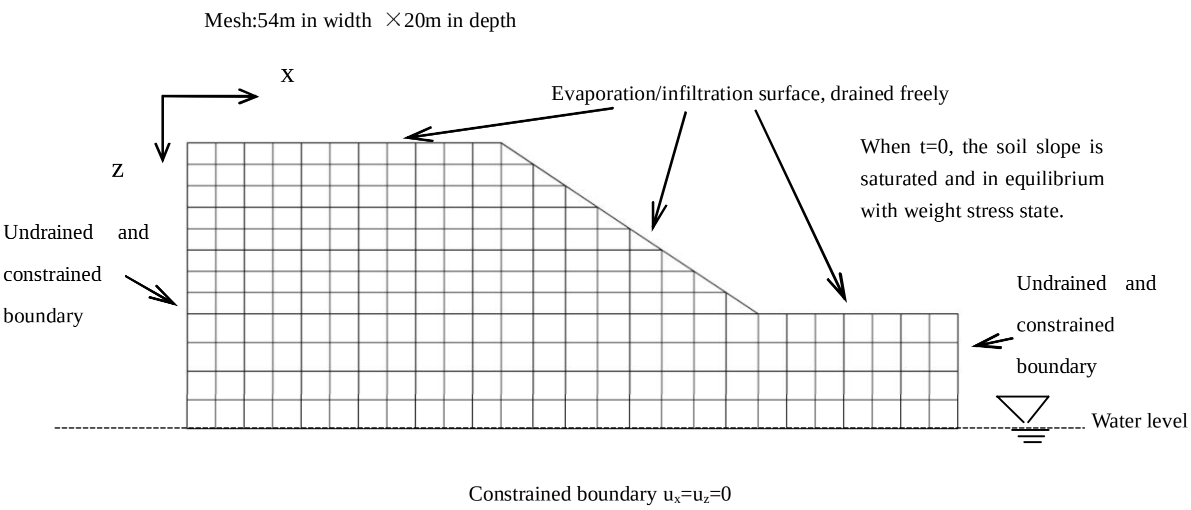

Fig.7(a). Computational mesh and boundary conditions

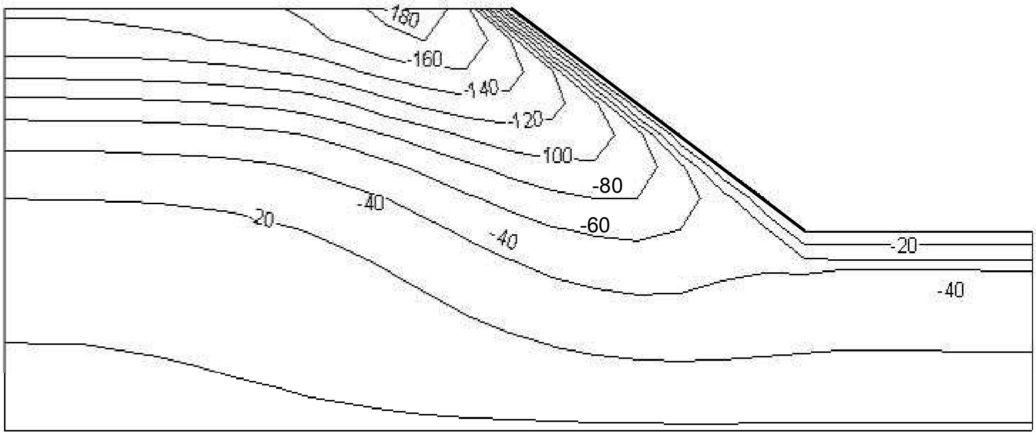

Fig.7 (b) Pore water pressure distribution at the end of evaporation (kPa)

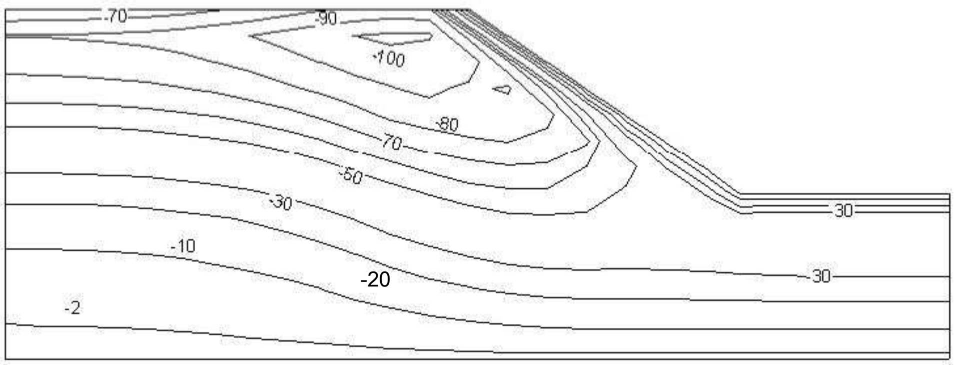

Fig.7 (c) Pore water pressure distribution at the end of infiltration (kPa)

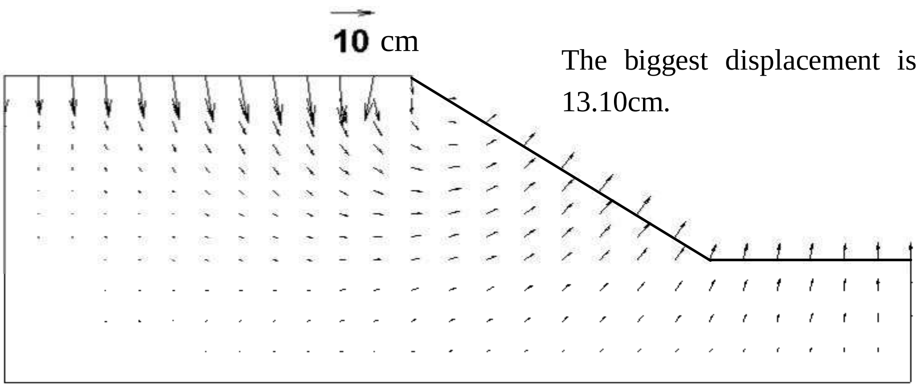

Fig.7 (d) Displacement distribution at the end of evaporation

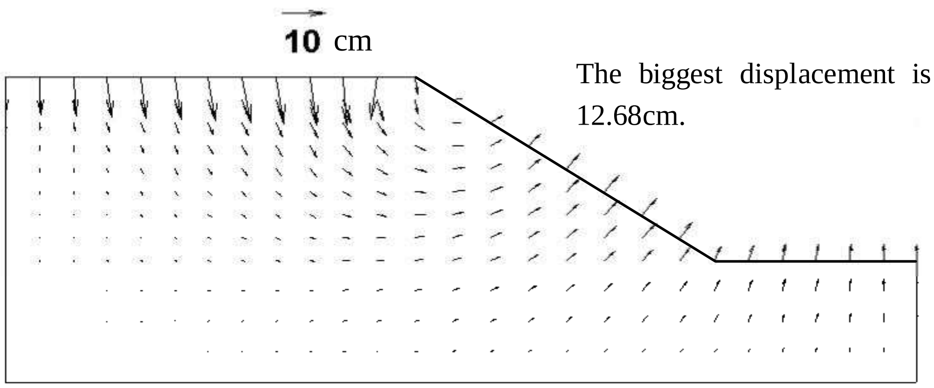

Fig.7 (e) Displacement distribution at the end of rainfall infiltration

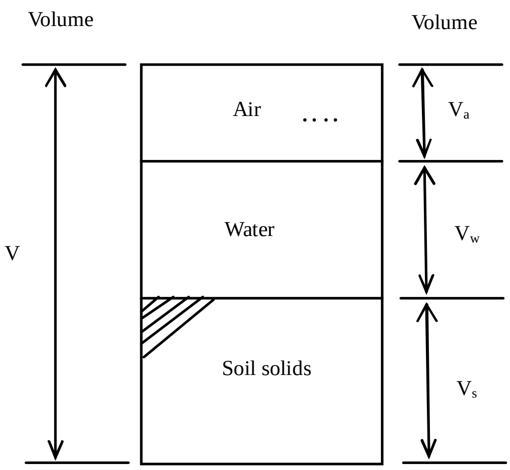

Fig.A1 Simplified three phase diagram